Eur. Phys. J. B **33**, 103–107 (2003)
DOI: 10.1140/epjb/e2003-00146-y

THE EUROPEAN PHYSICAL JOURNAL B

Vortex matter in lead nanowires

G. Stenuit[1,3,a], S. Michotte[2,3], J. Govaerts[1,3], and L. Piraux[2,3]

[1] Institut de Physique Nucléaire (FYNU), Université catholique de Louvain, Louvain-la-Neuve, Belgium
[2] Unité de Physico-Chimie et de Physique des Matériaux (PCPM), Université catholique de Louvain, Louvain-la-Neuve, Belgium
[3] Research Center on Microscopic and Nanoscopic Electronic Devices (CERMIN), Université catholique de Louvain, Louvain-la-Neuve, Belgium

Received 16 January 2003 / Received in final form 27 March 2003
Published online 23 May 2003 –

Abstract. Theoretical and experimental magnetizations of lead nanowire arrays well below the superconducting transition temperature T_c are described. The magnetic response of the array was investigated with a SQUID magnetometer. Hysteretic behaviour and phase transitions have been observed in sweeping up and down the external magnetic field at different temperatures. The Meissner and Abrikosov states were also experimentally observed in this apparently type-I superconductor. This fact brings to the fore the non-trivial behaviour of the critical boundary κ_c ($= 1/\sqrt{2}$ in bulk materials) between type-I and type-II phase transitions at mesoscopic scales. The time-independent Ginzburg-Landau equations particularized to cylindrically symmetric configurations enable one to explain and reproduce the experimental magnetization curves within 10% of error.

PACS. 74.25.Ha Magnetic properties – 74.20.De Phenomenological theories (two-fluid, Ginzburg-Landau, etc.) – 85.25.Kx Superconducting wires, fibers, and tapes

1 Introduction

Recent developments in nanotechnologies and measurement techniques allow nowadays the experimental investigation of the magnetic and thermodynamic superconducting properties of mesoscopic samples [1,2]. In order to compare the magnetization curves (magnetization *versus* external magnetic field at a given temperature T) of an array of lead nanowires to the theoretical predictions, a general understanding of the solutions to the Ginzburg-Landau (GL) theory must be achieved. In the present contribution, solutions to the GL equations are reported in this geometry, together with some explicit numerical examples compared to actual experimental data.

2 The Ginzburg-Landau equations

For time independent configurations in the absence of any external electric field, but in the presence of an external magnetic field $\boldsymbol{B}_{ext}$, the free energy of a superconductor reads

$$E = \int_{\infty} \mathrm{d}^3\boldsymbol{x} \frac{1}{2\mu_0} \left(\boldsymbol{B} - \boldsymbol{B}_{ext}\right)^2 + \int_{\infty} \mathrm{d}^3\boldsymbol{x} \frac{1}{2\mu_0} \left(\frac{\Phi_0}{2\pi\lambda^2}\right)^2 \lambda^2 \times \left\{ \left| \boldsymbol{\nabla}\Psi - \mathrm{i}\frac{q}{\hbar}\boldsymbol{A}\Psi \right|^2 + \frac{1}{2\xi^2}|\Psi|^2 \left[|\Psi|^2 - 2\right] \right\}, \quad (1)$$

where $\Psi(\boldsymbol{x})$ is the order parameter, or Cooper pair wave function, normalized to its constant value in the bulk of the material in the absence of magnetic field; $\boldsymbol{B}(\boldsymbol{x}) = \boldsymbol{\nabla} \times \boldsymbol{A}$, $q = -2|e| < 0$ is the Cooper pair charge, and $\lambda(T)$ and $\xi(T)$ are the penetration and coherence lengths, respectively. With this parametrization, the free energy vanishes at the normal-superconducting transition and remains negative when the sample is in the superconducting phase. From equation (1), the physical meaning of each contribution appears clearly: λ weighs the relative energetic contributions of the magnetic field and the condensate, while ξ weighs the relative contributions of the condensate energy due to spatial inhomogeneities in $\Psi(\boldsymbol{x})$ and deviations from the bulk value $|\Psi| = 1$ (GL potential energy).

Extremizing the free energy (1) leads to the GL equation

$$\lambda^2 \left[\boldsymbol{\nabla} - \mathrm{i}\frac{q}{\hbar}\boldsymbol{A}\right]^2 \Psi = \kappa^2 \Psi \left[|\Psi|^2 - 1\right] \quad (2)$$

which couples to Maxwell's equation,

$$\boldsymbol{\nabla} \times \boldsymbol{B} = \mu_0 \boldsymbol{J}_{em}, \quad (3)$$

with the electromagnetic current density given by

$$\mu_0 \boldsymbol{J}_{em} = \frac{\mathrm{i}}{2} \left(\frac{\Phi_0}{2\pi\lambda^2}\right) \times \left[\Psi^* \left(\boldsymbol{\nabla}\Psi - \mathrm{i}\frac{q}{\hbar}\boldsymbol{A}\Psi\right) - \left(\boldsymbol{\nabla}\Psi^* + \mathrm{i}\frac{q}{\hbar}\boldsymbol{A}\Psi^*\right)\Psi\right]. \quad (4)$$

[a] e-mail: stenuit@fynu.ucl.ac.be

Our numerical approximations are set up to simulate cylinder of infinite height immersed in an external magnetic field parallel to its axis ($\pm\hat{e}_z$ direction). Indeed, in the experiment, the external magnetic field is applied parallel to the nanowires axis to avoid demagnetization effects. Moreover, these nanowires are so long (50 μm) compared to the coherence length that they can be modelled as being infinite in height. It is well-known that the solutions to the GL equations for axially symmetric mesoscopic samples can be divided into two different classes [1,3–6].

In the first case, the order parameter $\Psi(\boldsymbol{x})$ is axially symmetric inside the material. Consequently, imposing this symmetry as well as invariance under translations along z, the functions being integrated in the free energy (1) are only radial dependent, except for the possible angular dependence of the phase of the order parameter. Therefore, under these symmetries, our numerical approach may be viewed as a one dimensional (1D) model. Indeed, applying the following parametrizations: $\boldsymbol{B} = B(r)\hat{e}_z$, $\boldsymbol{A} = A(r)\hat{e}_\phi$, $\mu_0 \boldsymbol{J}_{em} = J(r)\hat{e}_\phi$, $\Psi(r,\phi) = f(r)\mathrm{e}^{\mathrm{i}\theta(\phi)}$ and $\rho(r) = |\Psi(r,\phi)|^2 = f^2(r)$, the system of GL equations reduces to:

$$\begin{cases} \frac{\partial^2}{\partial u^2} g(u) = \frac{1}{u}\partial_u g(u) + f^2(u) g(u) \\ \frac{\partial^2}{\partial u^2} f(u) = -\frac{1}{u}\partial_u f(u) + \frac{1}{u^2} f(u) g^2(u) \\ +\kappa^2 f(u)\left(f^2(u) - 1\right) \end{cases} \tag{5}$$

where $u = \frac{r}{\lambda}$, $b(u) = \frac{B(u)}{\Phi_0/(2\pi\lambda^2)} = \frac{1}{u}\partial_u g(u)$ and $g(u) = u\frac{q\lambda^3}{\hbar}\frac{1}{f^2(u)}J(u)$ are properly normalized dimensionless variables.

The boundary conditions (b.c.) associated to this coupled system of nonlinear equations are
at $u = 0$:

$$\begin{cases} g(u)|_{u=0} = -L; \\ \partial_u f(u)|_{u=0} = 0 \text{ if } L = 0 \\ \text{or } f(u)|_{u=0} = 0 \text{ if } L \neq 0, \end{cases} \tag{6}$$

at $u = u_b$:

$$\begin{cases} \frac{1}{u}\partial_u g(u)|_{u=u_b} = b_{ext}; \\ \partial_u f(u)|_{u=u_b} = 0. \end{cases} \tag{7}$$

where L stands for the fluxoid quantum number, such that $\Psi(r,\phi) = f(r)\mathrm{e}^{-\mathrm{i}L\phi}$.

At each boundary, only two b.c. are specified whereas four such conditions are required for a unique solution. Hence, a numerical approach requires two more parameters, say f_0 and g_0, to be specified at one of the boundaries, with values to be adjusted such that the two other b.c. are met at the other boundary (shooting method).

Beyond the well-known solutions describing the Meissner (no vorticity, $L = 0$) and paramagnetic Meissner ($L \neq 0$) effects, solutions corresponding to ring-like current vortices (called "annular vortices") were found in cylindrical configurations with radius larger than the product $\pi\xi$ (see Ref. [7] for further details).

In the second case, the axial symmetry is broken. Multivortex [3] and half-integer vortex [8,9] states become therefore possible.

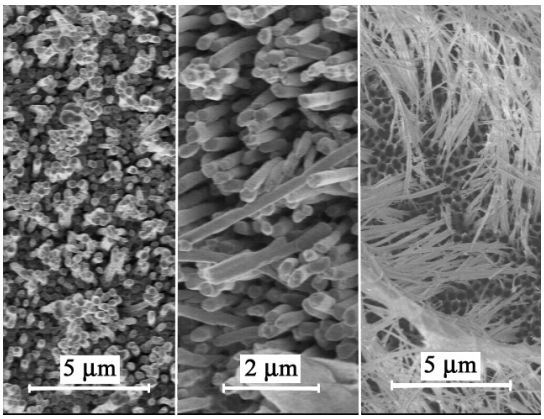

Fig. 1. From left to right: SEM micrographs showing three subsequent steps after 3, 6 and 9 minutes respectively of dissolution from the top of the membrane at room temperature.

3 Experimental and theoretical magnetization curves

Magnetization measurements of lead nanowires arrays were performed using a SQUID extractive magnetometer. The mesoscopic superconducting nanowires with large aspect ratio were grown by electrodeposition inside nanoporous anodized alumina membranes (see [2] for further details). Such a membrane contains a densely packed array of regular shaped pores (diameter around 250 nm) without lateral crossovers between individual pores. For the magnetic measurements, all the nanowires are kept inside the membrane so that they are all parallel to one another and to the applied magnetic field B_{ext}. Their large number produces a magnetization detectable by the SQUID and, due to the high penetration of the magnetic field inside the nanowires, their mutual interaction may be neglected. The membrane itself being paramagnetic, gives a signal that is one order of magnitude smaller than the magnetization of the nanowires, which may thus be easily subtracted (linear function of B_{ext}). Note that the cathode which is used for the electrodeposition [2] has been removed before performing measurements.

The array of lead nanowires has been observed using a SEM microscope. For this purpose, the membrane is partially dissolved from the top using a NaOH (5 mol/l) solution and rinsed with water. As a consequence (see Fig. 1), the nanowires are piled up and clearly display their large aspect ratio. On the right of the same figure, one can also see the relative regular shape of the pores (even though they are a bit enlarged by the dissolution). On the central part of the figure, the relatively good cylindrical geometry of these lead nanowires may also be noticed.

3.1 Magnetization modelling

In order to reproduce theoretically the total magnetization of the sample, some assumptions must be considered to simplify the model.

First of all, due to the small radius of the nanowires, only the 1D radial GL equations with $L = 0$ and, for the lowest temperatures, with $L = 1$, are used to explain the experimental magnetization. Indeed, for such sizes, temperatures and κ values, the phase diagram $(B_{ext}, Energy)$ exhibits only the states with $L < 2$ since the Giant Vortex (GV) states ($L \geq 2$) are too large compared to the radius.

In addition, the magnetization presents a weak diamagnetic (in the $L = 0$ state) and paramagnetic (in the $L = 1$ state) response in this mesoscopic limit. The mutual magnetic interactions between adjacent nanowires may thus be neglected in our model.

Therefore, considering a Gaussian distribution for the radii r_i of nanowires constituting the array, the total theoretical magnetization may be written as,

$$M_{tot} = A \sum_{r_i} \alpha(r_i)\, m(r_i), \tag{8}$$

where

- A is a scaling factor related to the number N of nanowires (with height h) inside the sample: $N = A/(h\Phi_0)$,
- $m(r_i)$ is the theoretical magnetization of one nanowire with radius r_i. Such quantity is obtained numerically (see Fig. 6, below) by using a shooting method with two point boundary value problems [10] to solve the 1D-GL equations (5),
- $\alpha(r_i) = \frac{1}{\sigma\sqrt{2\pi}} \mathrm{e}^{\frac{-(\bar{r}-r_i)^2}{2\sigma^2}}$ is the statistical weight associated to the magnetization $m(r_i)$, assuming a Gaussian distribution with mean radius $\bar{r}$ and variance σ^2,
- the summation extends over all radii from $\bar{r} - 3\sigma$ to $\bar{r} + 3\sigma$ with 1 nm steps.

3.2 Analysis of the experiments

The following analysis proposes a comparison between experimental magnetization curves of lead nanowires (critical temperature $T_c = 7.2$ K), with a mean radius of 116 nm and a variance of 11 nm[1]. These values being fixed, the free parameters of the model are λ, ξ and A. Finally, in order to study the hysteretic behaviour of the sample, it is worth mentioning here that the experimental magnetization curves have been obtained when the external magnetic field is swept up and down after a zero field cooling.

Figure 2 shows experimental and theoretical results for four values of the temperature close to T_c. Beyond the qualitative and quantitative agreement between the curves, it should be stressed that the absence of experimental hysteretic behaviour was also anticipated on basis of the model. Indeed, for such temperatures, the phase diagram $(B_{ext}, Energy)$ (see Fig. 6 with $T = 6.85$ K) exhibits a second-order phase transition near the critical magnetic field. In addition, we should recall that the critical magnetic field is enhanced compared to its bulk value because of the incomplete Meissner effect [2].

[1] The average radius and the variance could be determined by means of a scanning electronic microscope (SEM).

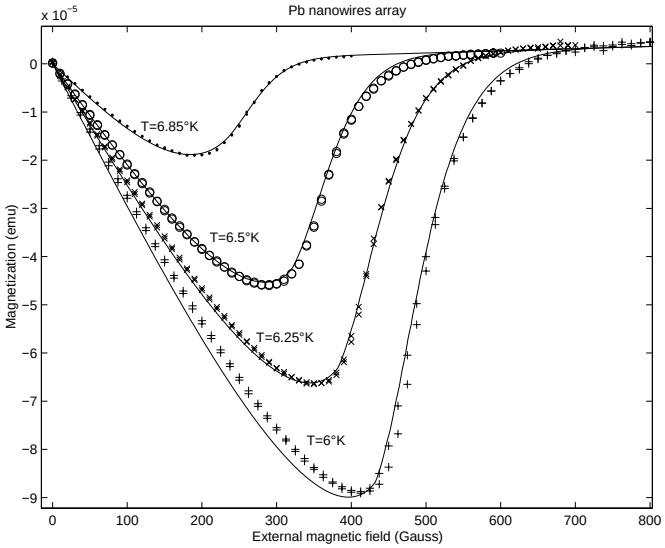

Fig. 2. Comparison between the experimental (markers) and theoretical (solid lines) total magnetization with $L = 0$. From top to bottom, curves at $T = 6.85$ K, $T = 6.5$ K, $T = 6.25$ K and $T = 6$ K respectively. The adjusted values for λ and ξ are $(\lambda, \xi) = (120, 260), (75, 197), (70, 168), (65, 152)$ nm respectively.

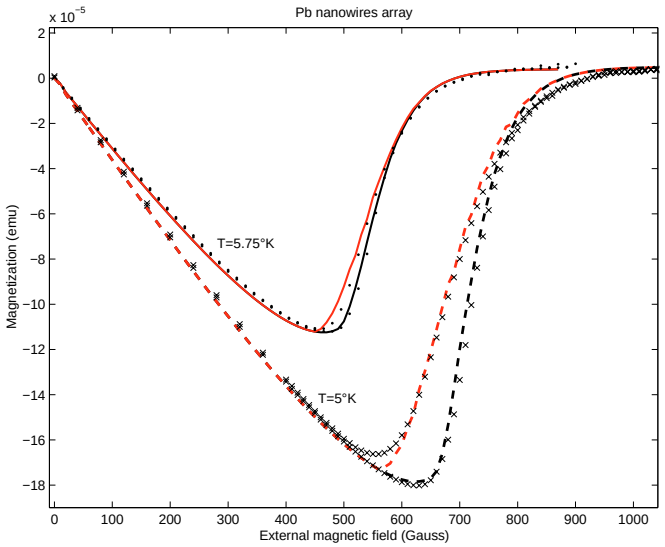

Fig. 3. Comparison between the experimental (markers) and theoretical (solid and dotted lines) total magnetization with $L = 0$. From top to bottom, curves at $T = 5.75$ K and $T = 5$ K. The adjusted values for λ and ξ are $(\lambda, \xi) = (58, 139), (51, 113)$ nm respectively.

For temperatures of $T = 5.75$ K and $T = 5$ K (see Fig. 3), the model predicts a first order phase transition with a jump in the magnetization and an hysteresis between the normal and superconducting states. Indeed, as shown in Figure 6 (in particular in the inset), the Meissner state ($L = 0$) exhibits a bistable region near the transition where the sample can be either superconducting or normal depending on the direction of the magnetic sweep. Considering a critical value B_t^{up} for the increasing magnetic

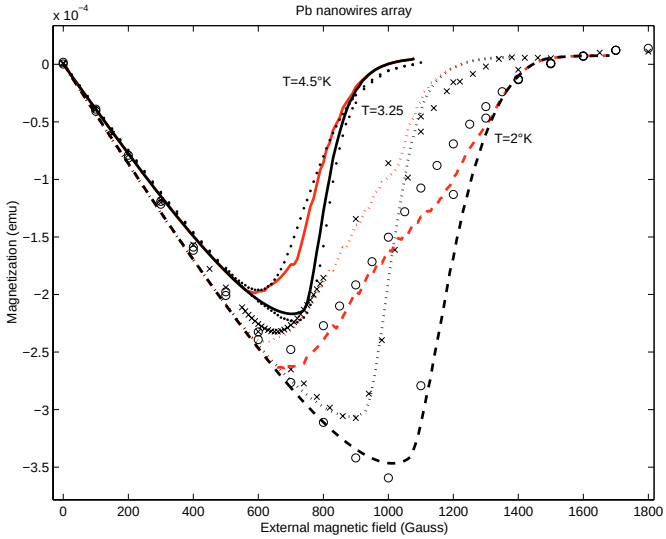

Fig. 4. Comparison between the experimental (markers) and theoretical (solid and dotted lines) total magnetization with $L = 0$ and $L = 1$. From top to bottom, curves at $T = 4.5$ K, $T = 3.25$ K and $T = 2$ K respectively. The adjusted values for λ and ξ are $(\lambda, \xi) = (51, 100), (48, 83), (48, 72)$ nm respectively.

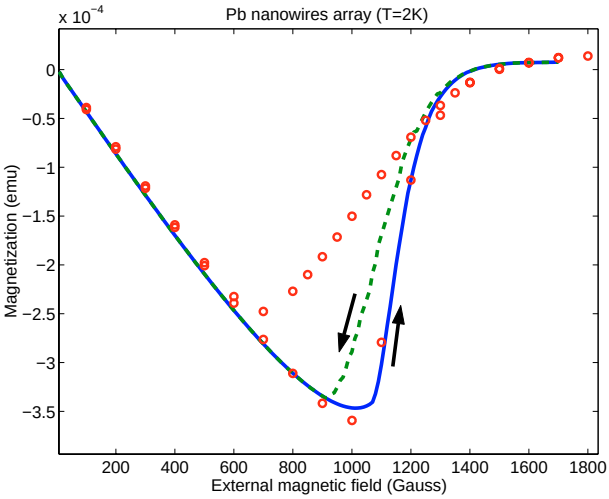

Fig. 5. Comparison between the experimental (markers) and theoretical (solid and dotted lines) total magnetization at $T = 2$ K with $L = 0$ only. The adjusted values for λ and ξ are $(\lambda, \xi) = (48, 72)$ nm. The arrows indicate the direction of the sweeping external magnetic field.

field at the superconducting-to-normal transition, and a critical value B_t^{down} for the decreasing magnetic field at the normal-to-superconducting transition, the theoretical curves fit the experimental data for the adjusted values of parameters λ and ξ specified in the figure caption. The absence of jumps in the transition is explained by the spread in values of the radii (high variance) of all nanowires constituting the sample. In the limit $\sigma \to 0$, a jump in the theoretical magnetization appears, as can be seen experimentally on a single disk [1].

For the three last temperatures studied experimentally (see Fig. 4), the Abrikosov state $L = 1$ extends the phase diagram $(B_{ext}, Energy)$ (see Fig. 6 with $T = 2$ K). Due to the Bean-Livingston barrier[2], the hysteretic behavior is enhanced and determined by the transition fields between $L = 0$ and $L = 1$ states (denoted $B^t_{L=0\to1}$ and $B^t_{L=1\to0}$). Since our numerical simulations fix the vorticity L, the values of the transition field were adjusted to fit the experiment. From the analysis, it follows that $B^t_{L=0\to1}$ lies close to the normal free energy of the $L = 0$ state and $B^t_{L=1\to0}$ lies close to the minimum of the free energy in the $L = 1$ state, as predicted in [13]. Without considering the $L = 1$ contribution, the experimental hysteretic behaviour and the critical field cannot be reproduced as displayed in Figure 5. We also note that the jump in the transition is replaced by a smooth monotonous curve because of non-negligible variance in the radii values.

Finally, Figure 7 shows the temperature dependence of the characteristic lengths λ and ξ, adjusted to fit the

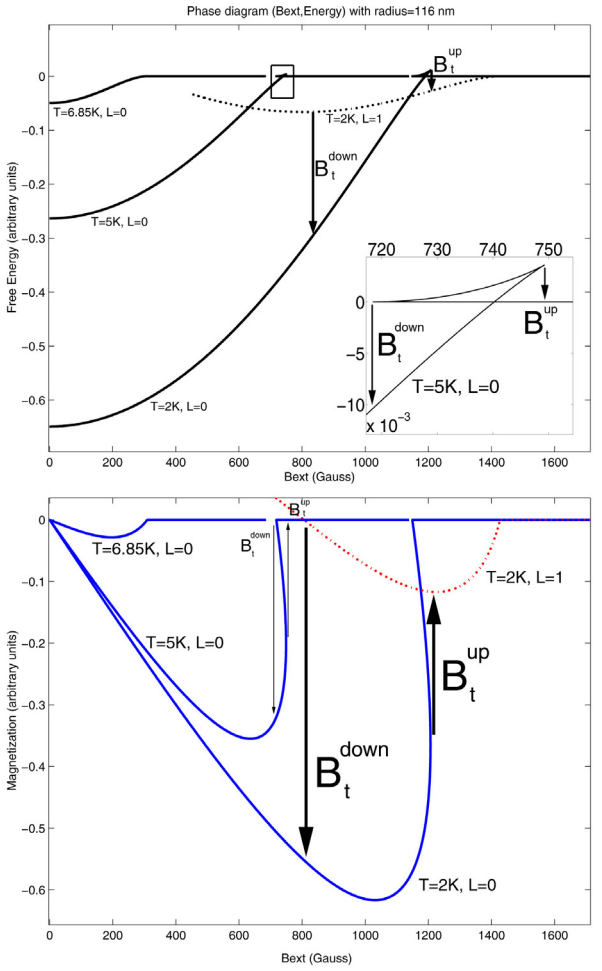

Fig. 6. The normalized free energy (above) and the magnetization (below) as function of the external magnetic field for $R = 116$ nm and $T = 6.85$, 5 and 2 kelvins. The inset in the above figure is a zooming of the boxed area which exhibits the hysteretic behavior of the free energy near the critical magnetic field at $T = 5$ K.

[2] This barrier is due to the fact that the superconducting current creating a magnetic vortex is running in a direction Opposite to that of the the screening current at the edge of the sample [11,12].

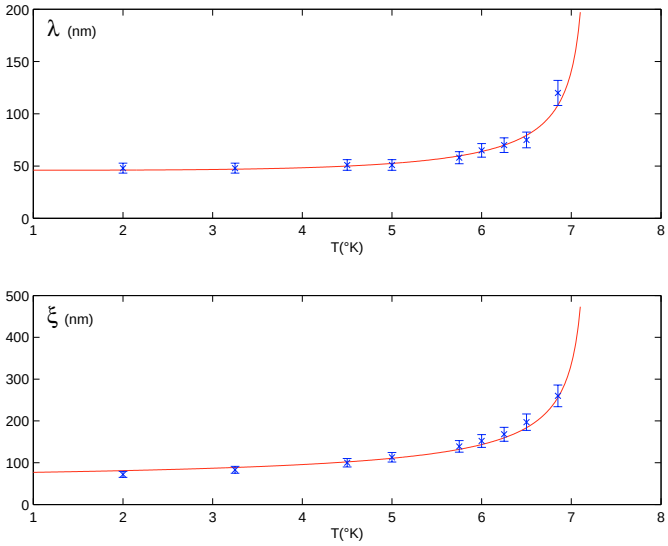

Fig. 7. The figure presents the temperature dependence of λ and ξ. The adjusted values (in order to fit the magnetization curves) are in agreement with the empirical laws (9) for $\lambda_0 =$ 46 nm and $\xi_0 = 74$ nm (solid lines). The error bars represent a 10% variation around the given value.

experiments. All values agree within 10% with the empirical laws [14],

$$\begin{cases} \lambda(T) = \frac{\lambda_0}{\sqrt{1-t^4}} & \text{where} \quad t = \frac{T}{T_c} \\ \xi(T) = \frac{\xi_0(1-0.25t)}{\sqrt{1-t}} \end{cases} \tag{9}$$

where, $\lambda_0 = 46$ nm and $\xi_0 = 74$ nm, *i.e.* almost the characteristic lengths of lead at zero temperature in the clean limit (mean free path $l \gg \lambda, \xi$). Although all the κ values ($= \lambda/\xi$) are below the critical one $\kappa_c = 1/\sqrt{2}$ (the lower figure), the penetration at low temperatures of one vortex is not surprising since the distinction between type-I and type-II looses its relevance at mesoscopic scales.

4 Comments and conclusions

In order to explain and reproduce within 10% of error the magnetic properties of our lead nanowires in an array, only the cylindrically symmetric solutions are required. In particular, the Meissner state ($L = 0$) and, for the lowest temperatures, the Abrikosov state ($L = 1$) were experimentally observed in these apparently type-I superconductors. The Giant Vortex states or the multivortex states with higher vorticity ($L \geq 2$) were not present since the size of such magnetic vortices is too large compared to the radius of the wires. However, the presence of an Abrikosov state is not surprising since the distinction between type-I and type-II looses its significance at mesoscopic scales. In particular, the critical boundary between type-I and type-II superconductor is not $\kappa_c = 1/\sqrt{2}$ (as in the case of a bulk material), but is a function of the normalized radius $u_b = \frac{R}{\lambda(T)}$ and the vorticity L of the cylinder, *i.e.* $\kappa_c = f(u_b, L)$ [15,12].

By changing the temperature of the sample in the SQUID magnetometer, we modified κ and also especially the normalized radius u_b. Consequently, we were able to check the three characteristic regions already observed by Geim *et al.* in another geometry (disk, see [1]): the type-II behaviour for small radius, the type-I phase transition in the Meissner state, and the vortex state with type-II phase transition from the superconducting to normal state. It should also be stressed that the absence of jumps in state transitions is explained by the spread in values of the radius of all nanowires within the sample.

This work provides thus a clear picture and a simple theoretical explanation for the magnetization of superconducting nanowire arrays close to and far away from the critical temperature, in perfect agreement with experiments.

G.S. is supported as a Scientific Collaborator of the "Fonds National de la Recherche Scientifique" (FNRS, Belgium). S.M. is a Research Fellow of the FNRS. This work has been partly supported by the Belgian Interuniversity Attraction Pole Program (PAI-IUAP P5/1/1) and by the "Communauté Française de Belgique" through the Program "Actions de Recherches Concertées".

References

1. A.K. Geim, I.V. Grigorieva, S.V. Dubonos, J.G.S. Lok, J.C. Maan, A.E. Filippov, F.M. Peeters, Nature **390**, 259 (1997)
2. S. Michotte, L. Piraux, S. Dubois, F. Pailloux, G. Stenuit, J. Govaerts, Physica C **377**, 267 (2002)
3. P. Singha Deo, V.A. Schweigert, F.M. Peeters, Phys. Rev. B **59**, 6039 (1999)
4. V.A. Schweigert, F.M. Peeters, Phys. Rev. Lett. **83**, 2409 (1999)
5. J.J. Palacios, Phys. Rev. B **58**, 5948 (1999)
6. W.V. Pogosov, Phys. Rev. B **65**, 224511 (2002)
7. J. Govaerts, G. Stenuit, D. Bertrand, O. Van der Aa, Phys. Lett. A **267**, 56 (2000)
8. J. Govaerts, J. Phys. A **34**, 8955 (2001) (`hep-th/0007112`)
9. G. Stenuit, J. Govaerts, D. Bertrand, *Half-Integer Number Vortices in the Ginzburg-Landau-Higgs Model*, edited by J. Annett, S. Kruchinin, NATO Science Series II, Vol. 67, pp. 375–384. (*Proceedings of the NATO Advanced Research Workshop "New Trends in Superconductivity", Yalta (Ukraine), September 16-20, 2001*)
10. W.H. Press, B.P. Flannery, S.A. Teukolsky, W.T. Vetterling, *Numerical Recipes: The Art of Scientific Computing* (Cambridge University Press, Cambridge, 1992)
11. C.P. Bean, J.B. Livingston, Phys. Rev. Lett. **12**, 14 (1964)
12. E. Akkermans, D. Gangardt, K. Mallick, Phys. Rev. B **62**, 12427 (2000)
13. B.J. Baelus, F.M. Peeters, V.A. Schweigert, Phys. Rev. B **63**, 144517 (2001)
14. M. Tinkham, *Introduction to Superconductivity*, 2nd edn. (McGraw-Hill, New York, 1996)
15. G.F. Zharkov, Phys. Rev. B **63**, 224513 (2001)